

First-principles prediction of pressure dependent mechanical, electronic, optical, and superconducting state properties of NaC_6 : A potential high- T_c superconductor

Nazmun Sadat Khan¹, B. Rahman Rano¹, Ishtiaque M. Syed¹, R. S. Islam², S. H. Naqib^{2,*}

¹Department of Physics, University of Dhaka, Dhaka-1000, Bangladesh

²Department of Physics, University of Rajshahi, Rajshahi-6205, Bangladesh

*Corresponding author e-mail: salehnaqib@yahoo.com

Abstract

Very recently carbon-rich NaC_6 with sodalite-like structure has been predicted to show high superconducting transition temperature above 100 K at relatively low applied (compared to high- T_c hydrides) hydrostatic pressures. We have investigated the pressure dependent structural, elastic, electronic, superconducting state, and optoelectronic properties of NaC_6 in this study. Some important thermophysical properties have also been explored. The elastic properties along with Poisson's and Pugh's ratios and optoelectronic parameters are investigated for the first time. NaC_6 was found to be structurally stable only at high pressures at and above 40 GPa, in agreement with previous study. The compound is highly ductile and the chemical bonding is prominently metallic in nature. The Debye temperature shows strong pressure dependence. The Grüneisen parameter also exhibits significant pressure dependence. The electronic band structure reveals metallic character and consists of highly dispersive and almost flat bands crossing the Fermi level. Both the electronic density of states at the Fermi level and repulsive Coulomb pseudopotential increase gradually with increasing pressure in the range 40 GPa to 70 GPa. The degree of dispersion in the $E(k)$ curves depend weakly on pressure both in the valence and conduction bands. The optical parameters spectra, studied for the first time, correspond well with the electronic band structure. NaC_6 absorbs and reflects electromagnetic radiation quite efficiently in the mid-ultraviolet region. Superconducting transition temperatures of NaC_6 have been estimated at different pressures and compared with previously reported values. The effects of various parameters on T_c have been discussed in details.

Keywords: High temperature superconductivity; Density functional theory (DFT); Structural properties; Optoelectronic properties; Effects of pressure on T_c

1. Introduction

The discovery of superconductors with high transition temperatures has attracted significant amount of research interest, both for its myriads of potential applications and the theoretical significance of the phenomenon [1–3]. However, a major stumbling block to its applications is the difficulty of achieving the conditions in which such a superconducting state can exist, namely requiring both high pressures and low temperatures. This is one of the primary reasons why there exists great interest in finding high- T_c superconductors under

external conditions conducive for practical applications. In this paper, high- T_c superconductors refer to those compounds other than the cuprates whose superconducting critical temperatures are at or above the boiling point of liquid nitrogen, meaning it could be cooled by relatively inexpensive coolants, as opposed to room temperature superconductors which have T_c at 0°C or above.

One of the earliest breakthroughs in this search was the theoretical prediction of high- T_c superconductivity of metallic hydrogen at very high pressures [4,5]. As of now, this superconductivity in metallic hydrogen has not been demonstrated, but it nevertheless inspired searches for high temperature superconductivity in hydrogen-rich compounds. A number of candidates have emerged such as H_3S , H_2S , CaH_6 , LaH_{10} and YH_{10} [6–8]. Recently, room-temperature superconductivity has been reported in carbonaceous sulfur hydride (CH_8S) [9]. Of the materials mentioned, YH_6 and YH_{10} are notable, because the hydrogen in those compounds form a sodalite-like structure [8]. Neil Ashcroft predicted on theoretical grounds that hydrogen under high external pressure will exhibit superconductivity, however the need for such external physical pressure might be alleviated by forming metallic hydrides where the hydrogen atoms are “pre-compressed” because of its chemical structure [4,10]. Prior research indicates this to be true for the case of CaH_6 , YH_6 and YH_{10} having sodalite-like hydrogen cage [7,11]. The nature of superconductivity in these materials is believed to be conventional, arising out of large electron-phonon coupling and very high Debye temperature.

Despite these advancements, the pressure requirements of these materials for superconductivity to manifest are still quite high. An alternative approach would be to replace H with C or other light elements in those sodalite structures. Superconductivity has been shown to occur in carbon compounds previously, such as boron-doped diamond, and of special significance to our work, in carbon compounds with similar sodalite structures [12–14]. From first-principles calculations, it has been shown that NaC_6 exhibits high critical temperature at around 100 K at relatively low pressures [12,13,15]. High electronic density of states and the presence of degenerate states near the Fermi level are significant contributors to a large electron-phonon interaction constant λ . The characteristic phonon energy is also high due to light mass of C atoms and high stiffness of the crystal lattice. All these contribute to the high T_c of NaC_6 . The material is stable at (comparatively) modest pressures which is desirable in a candidate for practical high- T_c superconductors.

In this work, we have conducted a thorough first-principles investigation of the physical properties of NaC_6 limited not only to its significance as a potential high- T_c superconductor, but also other properties of the material which have not been studied in any great depth till date. We have studied the bulk elastic properties of the material, Debye temperature, Grüneisen parameter, as well as its optical properties. The band structure and energy density of states have been analyzed. We have paid attention to the effect of pressure on the mechanical, electronic, and optical properties of this material. Potential applications of NaC_6 depend significantly on understanding these pressure dependent physical characteristics. As far as superconductivity itself is concerned, we have found that the large electron phonon coupling constant and high Debye temperature play a large part in the high

critical temperature of NaC_6 in fair agreement with the previous reports [12,13]. A detailed analysis of the pressure dependence of T_c has been carried out.

We have organized our manuscript as follows: In Section 2, we state the computation methodology used for all first principles calculations. In Section 3, we have tabulated and analyzed the results of the computations. We have discussed, in order, the crystal structure, the elastic properties, the Debye temperature, electronic band structure and energy density of states, optical properties and the critical temperature of the material under different pressures. In Section 4, we have summarized the key features and principal findings of our study.

2. Computational methodology

We have calculated the properties of NaC_6 from first principles calculations through Cambridge Serial Total Energy Package (CASTEP) [16]. Density Functional Theory (DFT) formalism is the basis on which the various properties of NaC_6 were derived. In DFT, instead of solving the many-body Schrödinger equation directly where the system is characterized by the complicated and difficult-to-compute electron wave functions, the problem is restated in terms of equivalent non-interacting problem where the system is described in terms of electron density. Solving the Kohn-Sham equations leads to the ground state density of the crystal system [17]. Both Local Density Approximation (LDA) and Generalized Gradient Approximation (GGA-PBE) were used as the exchange correlation functionals [18,19]. It is known that LDA tends to underestimate lattice parameters, while GGA sometimes overestimates those [16]. Ultra-soft pseudopotential, introduced by Vanderbilt, was used during the geometry optimization as it allows for lower basis cut-off, without sacrificing transferability too much [16,20]. Broyden–Fletcher–Goldfarb–Shanno (BFGS) algorithm was used to optimize the geometry of the crystal [21]. Pseudo atomic calculations were performed using the following electronic orbitals: C [$2s^2 2p^6$] and Na [$2s^2 2p^6 3s^1$]. The plane wave basis set cut-off energy has been set to 410 eV. A $6 \times 6 \times 6$ k -points mesh has been used based on Monkhorst-Pack scheme [22] for sampling the Brillouin zones (BZs) of NaC_6 . The system geometry was optimized under an energy tolerance of 5.0×10^{-6} eV/atom, maximum force tolerance of 0.01 eV/Å, maximum stress tolerance of 0.02 GPa and maximum displacement tolerance of 5.0×10^{-4} Å.

The single crystal elastic constants C_{ij} , bulk modulus B , shear modulus G were calculated from the *stress-strain* method contained in the CASTEP code. The electron energy dispersion and electronic energy density of states have been obtained from the optimized geometry of NaC_6 . The optical constants spectra were extracted from the estimated complex dielectric function, $\varepsilon(\omega) = \varepsilon_1(\omega) + i\varepsilon_2(\omega)$, which describes the frequency/energy dependent interactions of photons with the electrons in solids. Using the Kramers-Kronig transformations, the real part $\varepsilon_1(\omega)$ of dielectric function $\varepsilon(\omega)$ was calculated from the imaginary part $\varepsilon_2(\omega)$. The imaginary part, $\varepsilon_2(\omega)$, was calculated from the matrix elements of optical transitions between occupied and unoccupied electronic orbitals employing the CASTEP supported formula expressed as:

$$\varepsilon_2(\omega) = \frac{2e^2\pi}{\Omega\varepsilon_0} \sum_{k,v,c} |\langle \psi_k^c | \hat{u} \cdot \vec{r} | \psi_k^v \rangle|^2 \delta(E_k^c - E_k^v - E) \quad (1)$$

where, Ω is the volume of the unit cell, ω is angular frequency of the incident photon, e is the electronic charge, ψ_k^c and ψ_k^v are the wave functions of electrons in the conduction and valence band with a wave-vector k , respectively. The conditions of conservation of energy and momentum during the optical transition are ensured by the delta function in Eqn. 1. Once the real and imaginary parts of the dielectric function $\varepsilon(\omega)$ is known, all the other optical parameters such as refractive index, optical conductivity, reflectivity, absorption coefficient, and energy loss function can be computed from those [23]. The Debye temperature and other thermophysical parameters have been calculated from the elastic constants and elastic moduli of NaC_6 . All the properties mentioned here have been calculated in the pressure range from 0 GPa to 70 GPa with different pressure intervals.

3. Results and analysis

3.1. Crystal structure

The crystal structure of NaC_6 is cubic, belonging to the space-group $Im-3m$ (No-229), as shown schematically in Fig. 1. The Na atoms are embedded in a BCC lattice, surrounded by a characteristic cage (sodalite structure) of carbon atoms linked together through sp^3 bonds [12]. Each sodium atom is surrounded by 24 carbon atoms. The lattice parameters optimized under both GGA and LDA in the ground state are listed in Table 1. It is seen that the lattice parameters obtained by LDA are lower than those obtained using GGA, which is to be expected. The structural parameters obtained using GGA agree very well to those obtained in the previous study [12]. Since geometry optimization is a vital component in determining the reliability of *ab-initio* calculations we will focus mainly on results obtained via GGA in the sections to follow.

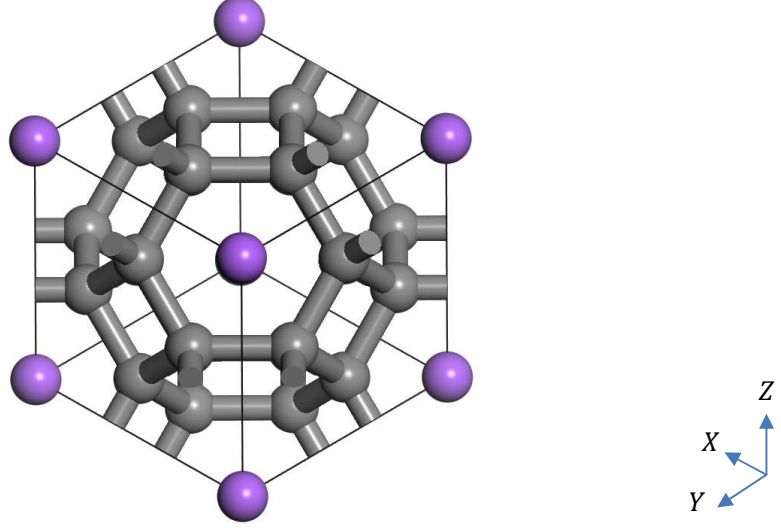


FIG. 1. Crystal structure of NaC_6 . The purple spheres represent the Na atoms at the corners and center of the cubic unit cell, and the grey spheres represent the C atoms forming the sodalite cage structure.

TABLE 1: The optimized lattice parameters and cell volumes of NaC_6 at 0 GPa obtained from GGA and LDA calculations. The lattice parameters a , b , and c are in \AA and the unit cell volume (V) is in \AA^3 .

Compound (functional)	a	b	c	V
NaC_6 (GGA)	4.563	4.563	4.563	95.026
NaC_6 (LDA)	4.499	4.499	4.499	91.092
NaC_6 (Theoretical [12])	4.570	4.570	4.570	95.443

3.2. Elastic properties

NaC_6 is predicted to have a high superconducting critical temperature for external pressures at and above 40 GPa. It is therefore, quite important to study the elastic and mechanical properties of the crystal to understand its behavior under high level of mechanical stress. The question of mechanical stability is also important. Because of the high degree of symmetry of cubic crystals, they only have three independent single crystal elastic constants namely, C_{11} , C_{12} and C_{44} . Stability of the crystal can be investigated via the Born criteria, as modified for cubic crystals [24,25]:

$$C_{11} - C_{12} > 0; C_{11} + 2C_{12} > 0; C_{44} > 0 \quad (1)$$

These are necessary and sufficient conditions of crystal stability under static stress. The obtained elastic constants at different values of hydrostatic pressure are given in Table 2.

TABLE 2: The single crystal elastic constants for NaC_6 (C_{ij} in GPa) calculated at various pressures (GPa).

Pressure (P)	C_{11}	C_{12}	C_{44}
0	783.20	69.86	-105.63
5	811.67	83.06	-121.56
10	838.29	96.34	-131.80
15	864.39	110.16	-134.44
20	890.21	124.62	-127.46
25	914.65	138.44	-103.86
29	934.03	150.01	-79.51
30	938.60	152.96	-73.51
31	943.78	155.64	-62.78
32	948.11	158.87	-58.11
33	952.73	161.85	-49.28
35	962.56	167.19	-31.39
40	985.68	181.95	7.80
50	1030.21	210.18	69.02
60	1073.93	238.01	102.62
70	1112.59	265.94	119.84

It is noted that the first two Born criteria are satisfied for all the pressures tested. However, the condition $C_{44} > 0$ is satisfied only for pressures close to 40 GPa and above. This indicates that NaC_6 is mechanically stable at and above 40 GPa. The phase stability of NaC_6 has been checked in the high pressure regions in Ref. [13]. A noticeable feature of the elastic constants is the extremely high values of the elastic constant C_{11} compared to the rest. The high value of elastic constant C_{11} ($C_{11} = C_{22} = C_{33}$) indicates strong resistance to tensile stress along the a , b , and c axes. This is also a clear signature of extreme anisotropy in bonding strength present in NaC_6 . The elastic constant C_{44} is a measure of resistance to shearing strain of the crystal. C_{44} ($C_{44} = C_{55} = C_{66}$) is significantly lower than C_{11} at all pressures, meaning that the material is far less resistant to shearing strain. The mechanical failure mode of NaC_6 is thus predicted to be controlled by shearing strain. The resistance of the crystal against volume conserving orthogonal distortion is determined by the constants C_{12} , C_{13} , C_{23} . In our case, the constant C_{12} ($C_{12} = C_{13} = C_{23}$) is lower as well, meaning the material displays weak resistance to orthogonal distortion. The Cauchy pressure, given by ($C_{12} - C_{44}$), is positive and high at all pressures, indicating the ductile nature [26] of NaC_6 .

The elastic moduli for bulk (polycrystalline) systems can be obtained from the single crystal elastic constants. These are listed in Table 3. The elastic moduli for bulk systems were calculated using the Voigt and Reuss approximations (indicated using subscripts V and R, respectively) [27,28]. These approximations provide upper and lower bounds of the parameters, respectively [29]. Hills approximations are the arithmetic mean of the respective Voigt and Reuss approximations, and, thus, provide a middle-ground between the two [30].

Besides the elastic moduli, Table 3 contains other important elastic indicators; the Poisson's ratio and the Pugh's ratio calculated at different pressures.

TABLE 3: The bulk moduli of the polycrystalline aggregates B_R, B_V, B_H (in GPa) and shear moduli G_R, G_V, G_H (in GPa), Young's moduli (E), Poisson's ratio (ν), and Pugh's ratio (B_V/G_V) under different pressures for NaC_6 . The subscripts R, V and H stand for Reuss, Voigt and Hills approximations, respectively.

Pressure (GPa)	B_R	B_V	B_H	G_R	G_V	G_H	E	ν	Pugh's ratio
31	418.28	418.35	418.32	-117.06	119.96	1.44	4.33	0.498	289.17
32	421.94	421.95	421.94	-107.39	122.98	7.79	23.23	0.490	54.13
33	425.44	425.48	425.46	-89.59	128.60	19.50	57.63	0.477	21.81
35	432.33	432.32	432.33	-55.22	140.23	42.50	123.47	0.452	10.17
40	449.84	449.86	449.85	12.84	165.43	89.13	250.84	0.407	5.04
50	483.51	483.52	483.52	103.42	205.41	154.42	418.68	0.355	3.13
60	516.63	516.65	516.64	146.98	228.75	187.87	502.68	0.337	2.75
70	548.15	548.16	548.15	168.02	241.23	204.63	545.96	0.334	2.67

For mechanically stable state under pressures of 40 GPa and above, the bulk modulus of NaC_6 is quite high and the sheer modulus is comparatively lower, indicating the material is more resistant to compression than shape deformation. With increasing pressure, both the bulk moduli and sheer moduli increases, the latter increasing quite sharply. The value of Poisson's ratio ν is quite high, close to the mathematical upper limit of 0.50, thus the material is highly incompressible [31,32]. With increasing pressure ν decreases, however for up to 70 GPa, it remains above 0.25, which indicates that the material is ductile in nature, supporting the analysis from the Cauchy pressures [33]. Large value of Poisson's ratio also implies that covalent bondings do not contribute significantly in the formation of NaC_6 [31,32]. Ductility, on the other hand, indicates that ionic/metallic bondings are prominent in this compound. Pugh's ratio [34] is a widely employed parameter to distinguish between brittle and ductile behaviors of solids. Solids with a Pugh's ratio of 1.75 or above exhibit ductility; solids possessing lower Pugh's ratio are expected to show brittleness [34-36]. The unrealistically high values of Pugh's ratio seen in Table 3 at pressures below 40 GPa stem from the fact that NaC_6 is elastically unstable for $P < 40$ GPa. The Young's modulus is a measure of the tensile strength of the material, which for an isotropic material can be calculated from bulk modulus and Poisson's ratio. From the table we see that the value of the Young's moduli increases with pressure, which can be explained by the increase of bulk modulus and decrease of Poisson's modulus with pressure. It is instructive to note that almost all the elastic parameters disclosed in Table 3 exhibit an abrupt change at pressure around 40 GPa. This is indicative of structural instability of the system at pressures below 40 GPa. It should be stressed that the results disclosed in Table 3 are novel and no prior estimates exist to compare.

3.3. Debye temperature and Grüneisen parameter

From the computed elastic moduli of the polycrystalline aggregates of NaC_6 , the Debye temperature θ_D can be calculated, at various pressures [37]. The Debye temperature is related to a number of important properties of the crystal and often arises in relation to specific heat, melting temperatures and phonon calculations. Furthermore, it is related to electron-phonon coupling constant and the critical temperature of superconductors. According to the Debye model, the Debye frequency ω_D is the highest allowed phonon frequency in crystal. The Debye temperature is related to ω_D by the formula $\theta_D = \hbar\omega_D/k_B$. The Debye temperature can be calculated from the average sound velocities as follows [37]:

$$\theta_D = \frac{h}{k_B} \left[\left(\frac{3n}{4\pi} \right) \frac{N_A \rho^{1/3}}{M} \right] v_m \quad (2)$$

where h is the Planck's constant, k_B is the Boltzmann's constant, n is the number of atoms in the molecule, N_A is the Avogadro's constant, ρ is the density, M is the molecular weight. The average sound velocity v_m is calculated by,

$$v_m = \left[\frac{1}{3} \left(\frac{2}{v_t^3} + \frac{1}{v_l^3} \right) \right]^{-\frac{1}{3}} \quad (3)$$

where v_t and v_l are the transverse and longitudinal elastic wave velocities, respectively. v_t and v_l can be further calculated from the polycrystalline elastic moduli as follows:

$$v_t = \left(\frac{G}{\rho} \right)^{\frac{1}{2}} \quad (4)$$

and

$$v_l = \left(\frac{B + \frac{4G}{3}}{\rho} \right)^{\frac{1}{2}} \quad (5)$$

The calculated values of ρ , v_l , v_t , v_m and Debye temperature θ_D are listed in Table 4. We see that the values of the Debye temperature are quite high and increases with increasing pressure. This contributes significantly to the high superconducting critical temperature of NaC_6 . The high values of θ_D is also an indication of the hardness of the material which agrees well with the elastic moduli from previous section.

TABLE 4: The density ρ in g/cm^3 , longitudinal (v_l), transverse (v_t) and average (v_m) elastic wave velocity in m/s, Debye temperature (θ_D) in K and the Grüneisen parameter (γ) for different pressures (in GPa), for the polycrystalline aggregate of NaC_6 .

Pressure	ρ	v_l	v_t	v_m	θ_D	γ
40	1.92	17174.97	6799.63	7704.76	1010.55	2.71
50	1.96	18708.53	8854.24	9962.58	1316.05	2.18
60	2.00	19539.28	9669.45	10853.80	1443.34	2.03
70	2.04	20024.77	9997.31	11216.11	1500.88	2.01

The crystal density of NaC_6 is very low. The Debye temperature and sound velocities increase rapidly with increase in the external pressure.

In addition to Debye temperature, we have calculated the Grüneisen parameter, γ , for NaC_6 at different pressures and presented those in Table 6. Grüneisen parameter is an important thermophysical indicator that gives a measure of lattice anharmonicity. A large value of γ implies high level of anharmonicity. The Grüneisen parameter was calculated from the computed values of Poisson's ratio using the following expression [38]:

$$\gamma = \frac{3(1 + \nu)}{2(2 - 3\nu)}$$

It is seen from Table that γ is quite large at 40 GPa. Further increase in pressure reduces the Grüneisen parameter.

3.4. Electronic band structure and energy density of states

The electronic band structure reveals a wealth of information about any material. The band structure plot (Fig. 2) shows the energies of the bands created by the overlap of energy levels of every atom in the crystal lattice at 40 GPa, along a path passing through certain high symmetry points of the Brillouin zone. The range of energies of the bands shown is from -10 eV to 10 eV, which contains the top of the valence bands and the bottom of the conduction bands. The Fermi level has been set at 0 eV. A fairly dispersive band of band width ~ 4.0 eV crosses the Fermi level along the path defined by X-R. This particular band exhibits hole-like dispersion. There are two more flat bands with electronic character running along M- Γ and Γ -R directions which also cross the Fermi level. The electrons belonging to these bands should have very large effective masses. The overall band structure of NaC_6 reveals clear metallic signatures at 40 GPa. The bands along R-M are less dispersive compared to the bands along M- Γ and Γ -R, that is to say they become more dispersive as we move towards the center of the Brillouin zone. With increasing pressure, the bands become more dispersive. At the high symmetry points Γ and R, we find a large number of degenerate electronic states. At the Γ point, some of these degenerate states reach and cross the Fermi Level, E_F . These degenerate states explain the high DOS around the Fermi level $N(E_F)$ found in the density of states calculations.

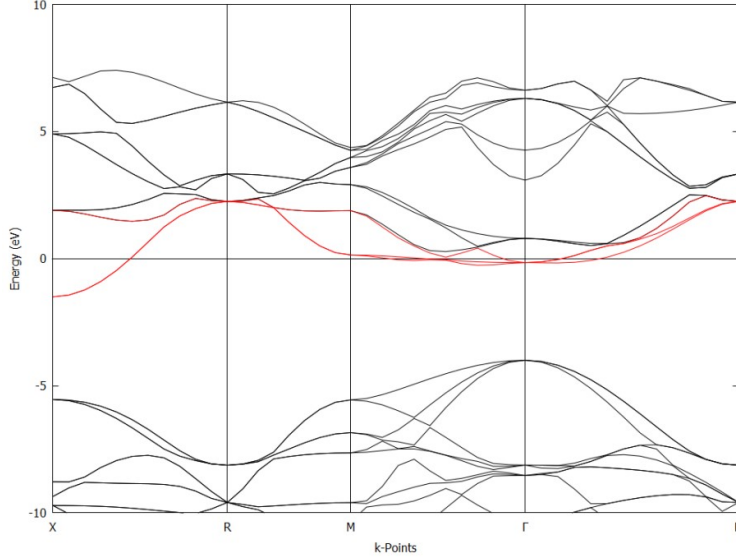


FIG. 2. The electronic band structure of NaC_6 along points of high symmetry (at 40 GPa) in the first Brillouin zone.

From the total density of states (TDOS) plot derived from the band structure of NaC_6 at 40 GPa shown in Fig. 3, it is clear that the density of states near the Fermi level, indicated by the vertical line at 0 eV, is quite high. This high value originates mainly from the nearly flat bands crossing the Fermi level. From the partial density of states (PDOS) calculated for the electronic orbitals of individual atoms, it is seen that most of the contribution towards TDOS comes from the C atoms, while Na atoms have almost no contribution below the Fermi level, and contribute very little at and above the Fermi level, which raises the TDOS slightly. From the DOS graph, the PDOS for C-2s and C-2p are comparable at the lower energy range, indicating that these electronic orbitals hybridize to form sp^3 covalent bonds. There is a presence of a shallow pseudogap in the neighborhood of E_F . In conventional metallic systems, the pseudogap often refers to the gap or valley between the bonding and anti-bonding peaks. This can occur for a number of reasons like charge transfer, covalence or d-resonance [39]. It should be stressed here that the weak pseudogap feature observed here is fundamentally different from that observed in hole doped high- T_c cuprate superconductors [40-42]. It is also worth noting that for materials having sodalite-like structures, charge transfer between constituent elements and carbon cage is an important contributor towards boosting T_c . The Na atoms donate almost all valence electrons to carbon. The presence of the pseudogap around the Fermi level has deep consequences for the nature of the material, such as its electronic stability [43,44]. Since E_F is located towards the right of the pseudogap, close to the antibonding region, NaC_6 displays a tendency to be in a disordered state. Figs. 2 & 3 only display the band structure and DOS features of NaC_6 at 40 GPa. We have calculated all these properties considering uniform hydrostatic pressures of 50 GPa, 60 GPa, and 70 GPa. At these pressures the compound under consideration is predicted to be structurally stable. Pressure dependent changes in the electronic band structure are monotonic and gradual, characterized by an increase in the electronic energy density of states at the Fermi level.

The TDOS at E_F , $N(E_F)$, is a vital parameter for superconductivity. It determines the electron-boson coupling strength [45,46], superconducting condensation energy [47,48], and the magnitude of the repulsive Coulomb pseudopotential, μ^* . This repulsive Coulomb term hinders the formation of Cooper pairs essential for superconductivity [45,46,49].

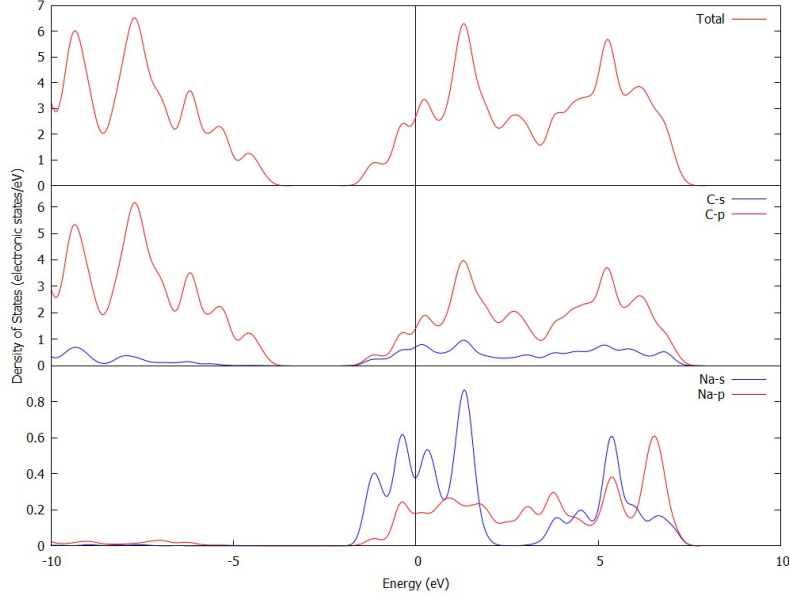


FIG. 3. The total and partial density of states of NaC_6 for 40 GPa external pressure.

We have summarized the effect of pressure on $N(E_F)$ and μ^* in Fig. 4. The Coulomb pseudopotentials at different pressures have been calculated following Refs. [50,51]. It is observed that both these parameters increase with increasing pressure. Compared to many other phonon-mediated superconductors, μ^* for NaC_6 is high [45].

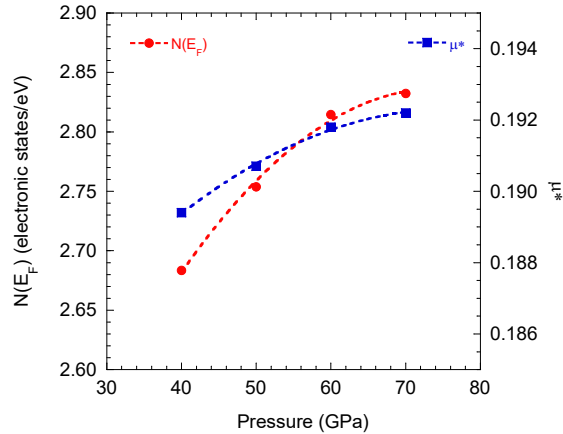


FIG. 4. The electronic density of states and repulsive Coulomb pseudopotentials of NaC_6 at different pressures. The dashed curves are second-order polynomial fits to the computed values.

Overall, the band structure features seen in this section agree quite well with those found in the previous studies [12,13].

3.5. Optical properties

A thorough study of optical parameters as a function of photon energy is important as these parameters describe the behavior of a material in response to incident electromagnetic radiation and are useful in determining the utility of the material in different optoelectronic applications. Besides, the optical parameters spectra are intimately related to the electronic band structure and their study yields complementary information related to fundamental physics. The optical parameters, namely, (a) the complex dielectric function, $\epsilon(\omega)$ (the real and imaginary parts), (b) refractive index $\eta(\omega)$, (c) optical conductivity $\sigma(\omega)$, (d) reflectivity $R(\omega)$, (e) absorption coefficient $\alpha(\omega)$ and (f) loss function $L(\omega)$ of NaC_6 have been calculated at different pressures. All these parameters were obtained by first determining the complex dielectric function. The CASTEP evaluates the imaginary part of the dielectric function using Eqn. 1 [52]. The real part of the dielectric function can then be found using Kramers-Kronig transform. From the dielectric functions, all other optical parameters can be obtained using standard formalism [53]. We have calculated optical parameters for all the pressures mentioned in Section 2. However, we have only disclosed the behaviors of energy dependent optical parameters at two representative pressures, 40 GPa and 60 GPa, in this section. Overall, the effect of pressure is moderate on the optical parameters. This is consistent with the computed electronic band structures where the effect of pressure was also found to be moderate.

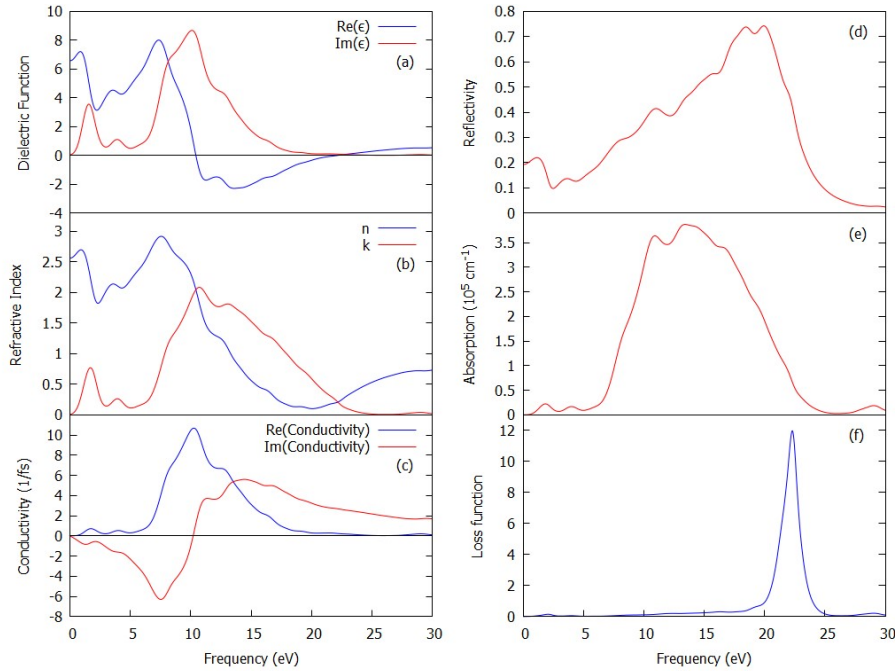


FIG. 5. The frequency dependent (a) dielectric function (real & imaginary parts), (b) refractive index (real & imaginary parts), (c) optical conductivity (real & imaginary parts), (d) reflectivity, (e) absorption coefficient, and (f) loss function of NaC_6 at 40 GPa.

Figures 5 and 6 illustrate the nature of the optical parameters at two different pressures. From Figure 5, at a pressure of 40 GPa, the dielectric function approaches zero after 22 eV energy, thus this is the plasma frequency of the material. After 22 eV, the material becomes nearly transparent since both the reflectivity and absorption coefficient falls sharply at this energy. The real part of the dielectric constant is a measure of polarization. For a certain range of energies from 10 eV to 22 eV, $R(\epsilon)$ is negative, implying that the polarization in response to incident electromagnetic fields acts to diminish it. The imaginary part, $\text{Im}(\epsilon)$, gives a measure of loss of incident energy within the system. The real part of the refractive index is the ratio of the speed of light in the medium to that in free space. The imaginary part of the refractive index is known as the extinction coefficient, which is related to the absorption coefficient. The real part of the refractive index is quite high for the light spectrum spanning infrared to ultraviolet range. After peaking at around 7 eV, it gradually diminishes at the plasma frequency 22 eV, after which it begins to rise briefly again. The conductivity links the current density to the electric field at various frequencies.

The reflectivity curve gradually rises from the infrared and visible light regions, but the value is rather low. However, starting from 10 eV (ultra violet region), it reaches a modest value of about 40% and continues to increase. We see that NaC_6 has high reflectivity approaching ~75% in the ultraviolet region encompassing 15 eV to 21 eV. This indicates that the material under consideration could have potential applications as ultraviolet reflector in this spectral band. The absorption coefficient follows the pattern of the extinction parameter as expected. The optical absorption coefficient is high over a wide spectral band (10 eV – 20 eV) in the ultraviolet region. The photon absorption efficacy of NaC_6 under high pressure is comparable to some other compounds [54-56] which have potential to be used as efficient ultraviolet absorber.

The loss function $L(\omega)$ shows a very sharp peak at 22 eV, which is the plasmon energy of the material. This is consistent with the fall of absorption and reflectivity functions around the same energy, which leads to the conclusion that the material is effectively transparent to the incident photons at and above the plasma frequencies.

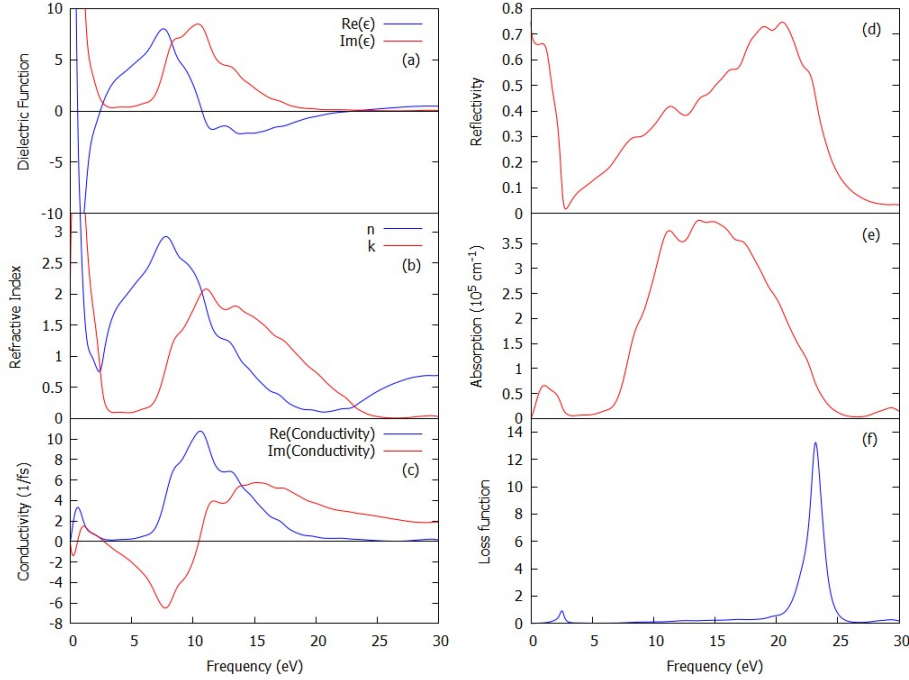


FIG. 6. The frequency dependent (a) dielectric function (real & imaginary parts), (b) refractive index (real & imaginary parts), (c) optical conductivity (real & imaginary parts), (d) reflectivity, (e) absorption coefficient, and (f) of NaC₆ at 60 GPa.

Increasing pressure gradually shifts the peak of the optical functions towards higher frequencies. Most of these optical properties retain the same general behavior for different frequencies under increasing pressure. However, starting from 50 GPa, the dielectric function, refractive index and the reflectivity undergoes some change, as seen in Figure 6 (showing optical parameters spectra for a pressure of 60 GPa). At 60 GPa, the optical parameters show sharper peaks at low energies in the dielectric constant, refractive index, and optical conductivity spectra. The dielectric function becomes high in the infrared range and decreases sharply towards the end of the visible light spectrum. After that, the dielectric function rises and displays the same general response as it did under lower pressures, and then flattens towards zero near the plasma frequency of approximately 23 eV. It reaches a peak value within 5-10 eV photon frequency. The same pattern is seen in that of refractive index and reflectivity, where they gain large peaks at low frequencies. Interestingly, the reflectivity is now high for visible light in addition to the 10 eV to 20 eV ultraviolet region with a sharp dip at ~ 4 eV in between. Further increase in pressure does not change the spectral features significantly other than small shifts in the peaks to higher energies including the peak in the loss function.

3.6. Pressure effects on superconductivity

Undoubtedly, the most significant property of NaC₆ is its predicted high superconducting critical temperature. The critical temperature of a strongly-coupled superconductor can be calculated using the widely employed McMillan formula [57]:

$$T_c = \frac{\theta_D}{1.45} \exp \left\{ -\frac{1.04(1 + \lambda)}{\lambda - \mu^*(1 + 0.62\lambda)} \right\} \quad (6)$$

where θ_D is the Debye temperature, λ is the electron phonon coupling constant and μ^* is the repulsive Coulomb pseudopotential. The values of these parameters and the critical temperature are enlisted in Table 5 together with the values obtained in Ref. [12]. Since CASTEP is unable to determine the Eliashberg spectral function [45], we have used the electron phonon coupling constants reported in a previous work [12] to determine T_c . The repulsive Coulomb pseudopotential has been calculated using the TDOS values at the Fermi level $N(E_F)$ obtained in this study, as follows [50]:

$$\mu^* = \frac{0.26N(E_F)}{1 + N(E_F)} \quad (7)$$

TABLE 5: Debye temperature θ_D in K, electron phonon coupling constant λ , density of states at Fermi Level $N(E_F)$ in states/eV, Coulomb pseudopotential μ^* , and critical temperature T_c in K at various pressures (GPa) for NaC₆.

Pressure (P)	θ_D	λ [12]*	$N(E_F)$	μ^*	T_c	T_c [12]*
40	1010.55	1.68	2.68	0.189	80.76	102.00
50	1316.05	1.58	2.75	0.190	97.44	101.00
60	1443.34	1.53	2.81	0.191	102.25	97.00
70	1500.88	1.50	2.83	0.192	103.50	95.00

*Some of these values are interpolated from the $T_c(P)$ and $\lambda(P)$ curves given in Ref. [12].

We can see from Table 5 that the calculated values of T_c at different pressures agree reasonably well with those found in Ref. [12]. Notable deviation is found for the values at 40 GPa, which we believe is due to the use of low value of μ^* in earlier works [12,13]. As mentioned in a previous section, repulsive Coulomb interaction reduces T_c since it reduces the effective electron-phonon interaction essential for the formation of phase coherent Cooper pairs. In earlier studies μ^* was taken ad-hoc to be in the range 0.10 – 0.13. If we take $\mu^* = 0.13$ and keep all other parameters unchanged the predicted T_c turns out to be 97.16 K very close to the value (102 K) obtained by Lu et al. [12].

There are several interesting features in the predicted $T_c(P)$ which needs elaboration. We have found that $N(E_F)$ increases gradually with increasing pressure. For conventional superconductors, the electron-phonon coupling constant $\lambda = N(E_F)V_{e-ph}$, where V_{e-ph} is the electron-phonon interaction energy [45]. On the other hand, λ decreases with increasing pressure [12,13]. This implies that even though $N(E_F)$ increases with pressure, V_{e-ph} decreases at a greater rate with increasing pressure, the overall effect is a pressure induced decrement of λ . This decrement can, at least partly, be explained considering the anharmonicity and softening of phonon modes in NaC₆. It is observed in Table 4 that the Grüneisen parameter (γ) is high at 40 GPa and decreases with increasing pressure suggesting that lattice anharmonicity and soft-phonon modes are diminished as pressure increases. This

is also supported by the increase in the Debye temperature with increasing pressure (Table 4). There is significant evidence that the electron-phonon coupling constant is enhanced in the presence of soft-phonon modes [58]. This observation follows from the pioneering work by Hopfield [59]. In terms of the Hopfield parameter, η , the electron-phonon coupling constant can be expressed as, $\lambda \sim \eta/\langle\theta^2\rangle$ [59]; $\langle\theta^2\rangle$ is the average squared phonon frequency expressed in temperature showing that presence of soft-phonon modes raises λ . Furthermore, the Debye temperature increases significantly with pressure but the effect of this increment is insignificant on the predicted values of T_c . This is indicative that the positive contribution of $\theta_D(P)$ to $T_c(P)$ is counterbalanced by the negative contribution due to decreasing $\lambda(P)$ and increasing $\mu^*(P)$ as pressure is increased. Similar arguments have been put forward to explain the predicted $T_c(P)$ behavior in recent studies [12,13].

4. Conclusions

On the basis of DFT based first-principles calculations we have carried out an investigation of the structural, elastic, electronic, optical, thermophysical and superconducting state properties of binary NaC_6 compound in the sodalite-like structure over a wide range of pressure. The compound is found to be elastically stable only for pressures at and above 40 GPa. In the stable phase NaC_6 possesses significant bonding anisotropy. The compound is predicted to be highly ductile and machinable with dominant ionic/metallic bondings. The electronic band structure reveals metallic features in agreement with previous studies [12,13]. The electronic density of states at the Fermi level and the Coulomb pseudopotential are found to increase with increasing pressure. The Debye temperature also increases with pressure. The Grüneisen parameter, on the other hand, decreases with increasing pressure in the elastically stable phase. NaC_6 is predicted to be an efficient absorber of electromagnetic radiation in the mid-ultraviolet region. At high pressures, the compound is also a good reflector of visible light. The superconducting transition temperature has been computed at different pressures and discussed in terms of the pressure induced variations in $N(E_F)$, λ , θ_D , and γ .

We hope that this study will inspire the researchers to study similar carbon-rich compounds in the sodalite-like structure in greater details in near future.

Acknowledgements

N. S. K. acknowledges the Research Fellowship from Semiconductor Technology Research Centre, University of Dhaka, Bangladesh, S. H. N. and R. S. I. acknowledge the research grant (1151/5/52/RU/Science-07/19-20) from the Faculty of Science, University of Rajshahi, Bangladesh, which partly supported this work.

Data availability

The data sets generated and/or analyzed in this study are available from the corresponding author on reasonable request.

Author Contributions

M. S. K. performed the theoretical calculations, contributed to the analysis and draft manuscript writing. B. R. R. performed the theoretical calculations, contributed to the analysis, and contributed to manuscript writing. I. M. S. supervised the project and contributed to finalizing the manuscript. R. S. I. contributed to analysis and manuscript writing. S. H. N. designed and supervised the project, analyzed the results and finalized the manuscript. All the authors reviewed the manuscript.

Competing Interests

The authors declare no competing interests.

References

- [1] J. W. Bray, *Superconductors in Applications; Some Practical Aspects*, IEEE Trans. Appl. Supercond. **19**, 2533 (2009).
- [2] J. R. Hull and M. Murakami, *Applications of Bulk High-Temperature Superconductors*, Proc. IEEE **92**, 1705 (2004).
- [3] R. C. Hansen, *Antenna Applications of Superconductors*, IEEE Trans. Microw. Theory Tech. **39**, 1508 (1991).
- [4] N. W. Ashcroft, *Metallic Hydrogen: A High-Temperature Superconductor?*, Phys. Rev. Lett. **21**, 1748 (1968).
- [5] J. M. McMahon and D. M. Ceperley, *High-Temperature Superconductivity in Atomic Metallic Hydrogen*, Phys. Rev. B **84**, 144515 (2011).
- [6] Y. Li, J. Hao, H. Liu, Y. Li, and Y. Ma, *The Metallization and Superconductivity of Dense Hydrogen Sulfide*, J. Chem. Phys. **140**, 174712 (2014).
- [7] H. Wang, J. S. Tse, K. Tanaka, T. Iitaka, and Y. Ma, *Superconductive Sodalite-like Clathrate Calcium Hydride at High Pressures*, Proc. Natl. Acad. Sci. U. S. A. **109**, 6463 (2012).
- [8] H. Liu, I. I. Naumov, R. Hoffmann, N. W. Ashcroft, and R. J. Hemley, *Potential High- T_c Superconducting Lanthanum and Yttrium Hydrides at High Pressure*, Proc. Natl. Acad. Sci. U. S. A. **114**, 6990 (2017).
- [9] E. Snider, N. Dasenbrock-Gammon, R. McBride, M. Debessai, H. Vindana, K. Vencatasamy, K. V. Lawler, A. Salamat, and R. P. Dias, *Room-Temperature Superconductivity in a Carbonaceous Sulfur Hydride*, Nature **586**, 373 (2020).
- [10] N. W. Ashcroft, *Hydrogen Dominant Metallic Alloys: High Temperature Superconductors?*, Phys. Rev. Lett. **92**, 1 (2004).
- [11] C. Heil, S. Di Cataldo, G. B. Bachelet, and L. Boeri, *Superconductivity in Sodalite-like Yttrium Hydride Clathrates*, Phys. Rev. B **99**, 1 (2019).
- [12] S. Lu, H. Liu, I. I. Naumov, S. Meng, Y. Li, J. S. Tse, B. Yang, and R. J. Hemley, *Superconductivity in Dense Carbon-Based Materials*, Phys. Rev. B **93**, 104509 (2016).
- [13] K. Sano, Y. Masuda, and H. Ito, *Superconductivity of Carbon Compounds with Sodalite Structure*, arXiv:2002.02174 (2020).
- [14] E. A. Ekimov, V. A. Sidorov, E. D. Bauer, N. N. Mel'nik, N. J. Curro, J. D.

- Thompson, and S. M. Stishov, *Superconductivity in Diamond*, Nature **428**, 542 (2004).
- [15] A. P. Drozdov, M. I. Eremets, I. A. Troyan, V. Ksenofontov, and S. I. Shylin, *Conventional superconductivity at 203 kelvin at high pressures in the sulfur hydride system*, Nature **525**, 73 (2015).
- [16] S. J. Clark, M. D. Segall, C. J. Pickard, P. J. Hasnip, M. I. J. Probert, K. Refson, and M. C. Payne, *First Principles Methods Using CASTEP*, Zeitschrift Fur Krist. **220**, 567 (2005).
- [17] W. Kohn and L. J. Sham, *Self-Consistent Equations Including Exchange and Correlation Effects*, Phys. Rev. **140**, A1133 (1965).
- [18] J. P. Perdew, K. Burke, and M. Ernzerhof, *Generalized Gradient Approximation Made Simple*, Phys. Rev. Lett. **77**, 3865 (1996).
- [19] J. P. Perdew and A. Zunger, *Self-Interaction Correction to Density-Functional Approximations for Many-Electron Systems*, Phys. Rev. B **23**, 5048 (1981).
- [20] D. Vanderbilt, *Soft Self-Consistent Pseudopotentials in a Generalized Eigenvalue Formalism*, Phys. Rev. B **41**, 7892 (1990).
- [21] C. G. Broyden, *The Convergence of a Class of Double-Rank Minimization Algorithms I. General Considerations*, IMA J. Appl. Math. (Institute Math. Its Appl. **6**, 76 (1970).
- [22] H. J. Monkhorst and J. D. Pack, *Special points for Brillouin-zone integrations*, Phys. Rev. B. **13**, 5188 (1976).
- [23] M. Benzineb, F. Chiker, H. Khachai, H. Meradji, Ş. Uğur, S. H. Naqib, S. Bin Omran, Xiaotian Wang, R. Khenata, *A comparative study of structural, thermal, and optoelectronic properties between zircon and scheelite type structures in SrMoO₄ compound: An ab-initio study*, Optik **238**, 166714 (2021).
- [24] M. Born, *On the Stability of Crystal Lattices. I*, Math. Proc. Cambridge Philos. Soc. **36**, 160 (1940).
- [25] F. Mouhat and F. X. Coudert, *Necessary and Sufficient Elastic Stability Conditions in Various Crystal Systems*, Phys. Rev. B - Condens. Matter Mater. Phys. **90**, 0 (2014).
- [26] D. G. Pettifor, *Theoretical Predictions of Structure and Related Properties of Intermetallics*, Mater. Sci. Technol. (United Kingdom) **8**, 345 (1992).
- [27] W. Voigt, *Lehrbuch Der Kristallphysik* (Vieweg + Teubner Verlag, 1966).
- [28] A. Reuss, *Berechnung Der Fließgrenze von Mischkristallen Auf Grund Der Plastizitätsbedingung Für Einkristalle .*, ZAMM - J. Appl. Math. Mech./Zeitschrift Für Angew. Math. Und Mech. **9**, 49 (1929).
- [29] P. Ravindran, L. Fast, P. A. Korzhavyi, B. Johansson, J. Wills, and O. Eriksson, *Density Functional Theory for Calculation of Elastic Properties of Orthorhombic Crystals: Application to TiSi₂*, J. Appl. Phys. **84**, 4891 (1998).
- [30] R. Hill, *The Elastic Behaviour of a Crystalline Aggregate*, Proc. Phys. Soc. Sect. A **65**, 349 (1952).
- [31] P. H. Mott, J. R. Dorgan, and C. M. Roland, *The Bulk Modulus and Poisson's Ratio of "Incompressible" Materials*, J. Sound Vib. **312**, 572 (2008).
- [32] G. N. Greaves, A. L. Greer, R. S. Lakes, and T. Rouxel, *Poisson's Ratio and Modern Materials*, Nature Materials **10**, 823 (2011).
- [33] M. I. Naher and S. H. Naqib, *A comprehensive study of the thermophysical and optoelectronic properties of Nb₂P₅ via ab-initio technique*, Results in Physics **28**,

- 104623 (2021).
- [34] S. F. Pugh, XCII. *Relations between the elastic moduli and the plastic properties of polycrystalline pure metals*, London, Edinburgh, Dublin Philos. Mag. J. Sci. **45**, 823 (1954).
- [35] M. M. Hossain and S. H. Naqib, *Structural, elastic, electronic, and optical properties of layered $TiNX$ ($X = F, Cl, Br, I$) compounds: a density functional theory study*, Molecular Physics **118** (3), e1609706 (2020).
- [36] M. A. Hadi, M. A. Rayhan, S. H. Naqib, A. Chroneos and A. K. M. A. Islam, *Structural, elastic, thermal and lattice dynamic properties of new 321 MAX phases*, Computational Materials Science **170**, 109144 (2019).
- [37] O. L. Anderson, *A Simplified Method for Calculating the Debye Temperature from Elastic Constants*, J. Phys. Chem. Solids **24**, 909 (1963).
- [38] G. A. Slack, *The Thermal Conductivity of Nonmetallic Crystals*, in: Solid State Phys. - Adv. Res. Appl., 1979: pp. 1–71.
- [39] C. D. Gelatt, A. R. Williams, and V. L. Moruzzi, *Theory of Bonding of Transition Metals to Nontransition Metals*, Phys. Rev. B **27**, 2005 (1983).
- [40] S. H. Naqib, J. R. Cooper, J. L. Tallon and C. Panagopoulos, *Temperature dependence of electrical resistivity of high- T_c cuprates - from pseudogap to overdoped regions*, Physica C: Superconductivity **387** (3-4), 365 (2003).
- [41] S. H. Naqib, J. R. Cooper, J. L. Tallon, R. S. Islam and R. A. Chakalov, *Doping phase diagram of $Y_{1-x}Ca_xBa_2(Cu_{1-y}Zn_y)_3O_{7-\delta}$ from transport measurements: Tracking the pseudogap below T_c* , Phys. Rev. B **71**, 054502 (2005).
- [42] R. S. Islam and S. H. Naqib, *Effects of Zn on magnetic properties and pseudogap of optimally doped $La_{2-x}Sr_xCuO_4$* , Physica C **470**, 79 (2010).
- [43] F. Parvin and S. H. Naqib, *Pressure dependence of structural, elastic, electronic, thermodynamic, and optical properties of van der Waals-type $NaSn_2P_2$ pnictide superconductor: Insights from DFT study*, Results Phys. **21**, 103848 (2021).
- [44] P. Ravindran and R. Asokamani, *Correlation between Electronic Structure, Mechanical Properties and Phase Stability in Intermetallic Compounds*, Bulletin in Materials Science **20**, 613 (1997).
- [45] J. P. Carbotte, *Properties of boson-exchange superconductors*, Rev. Mod. Phys. **62**, 1027 (1990).
- [46] A. K. M. A. Islam and S. H. Naqib, *Possible explanation of high- T_c in some 2D cuprate superconductors*, J. Phys. Chem. Solids **58**, 1153 (1997).
- [47] S. H. Naqib and R. S. Islam, *Possible quantum critical behavior revealed by the critical current density of hole doped high- T_c cuprates in comparison to heavy fermion superconductors*, Scientific Reports **9**, 1 (2019).
- [48] Nazir Ahmad and S. H. Naqib, *Estimation of Cooper pair density and its relation to the critical current density in $Y(Ca)BCO$ high- T_c cuprate superconductors*, Results in Physics **17**, 103054 (2020).
- [49] M. M. Mridha and S. H. Naqib, *Pressure dependent elastic, electronic, superconducting, and optical properties of ternary barium phosphides (BaM_2P_2 ; $M = Ni, Rh$): DFT based insights*, Physica Scripta **95** (10), 105809 (2020).
- [50] *Superconductivity in d- and f-Band Metals*, Ed. D. Douglass (Springer US, 1976).

- [51] M. I. Naher, M. A. Afzal and S. H. Naqib, *A comprehensive DFT based insights into the physical properties of tetragonal superconducting Mo_5PB_2* , Results in Physics **28**, 104612 (2021).
- [52] Material Studio, *CASTEP Guide*, Mater. Stud. 1 (2014).
- [53] M. M. Hossain, M. A. Ali, M. M. Uddin, S. H. Naqib and A. K. M. A. Islam, *Newly synthesized 3D boron-rich chalcogenides $B_{12}X$ ($X = S, Se$): Theoretical characterization of physical properties for optoelectronic and mechanical applications*, arXiv:2108.08493 (2021).
- [54] M. I. Naher and S. H. Naqib, *An ab-initio study on structural, elastic, electronic, bonding, thermal, and optical properties of topological Weyl semimetal TaX ($X = P, As$)*, Scientific Reports **11**, 5592 (2021).
- [55] M. A. Afzal and S. H. Naqib, *A DFT based first-principles investigation of optoelectronic and structural properties of Bi_2Te_2Se* , Physica Scripta **96**, 045810 (2021).
- [56] M. I. Naher and S. H. Naqib, *Structural, elastic, electronic, bonding, and optical properties of topological $CaSn_3$ semimetal*, Journal of Alloys and Compounds **829**, 154509 (2020).
- [57] W. L. McMillan, *Transition Temperature of Strong-Coupled Superconductors*, Phys. Rev. **167**, 331 (1968).
- [58] *Anharmonic Properties of High- T_c Cuprates*, Eds. D. Mihailovic, G. Runai, E. Kaldis, K. A. Muller, World Scientific (1994).
- [59] J. J. Hopfield, *Angular Momentum and Transition-Metal Superconductivity*, Phy. Rev. **186**, 443 (1969).